ChemComm

COMMUNICATION

View Article Online
View Journal | View Issue

Cite this: *Chem. Commun.*, 2025, **61**, 1625

Received 16th November 2024,
Accepted 13th December 2024

DOI: 10.1039/d4cc06100d

rsc.li/chemcomm

Photocatalytic reductive coupling of furfural into deoxyfuroin on mesoporous TiO_2†

Beibei Gao,[a] Shuxian Wang,[a] Min Liu,[b] Jialing Ma,[a] Tianliang Lu *[b] and Hongji Li *[a]

The two-step photocatalytic transformation of furfural into deoxyfuroin was achieved *via* the initial homocoupling of furfural into furoin over mesoporous TiO_2, followed by photocatalytic transfer hydrogenolysis of C–OH of furoin over the Cu/TiO_2 hybrid system.

Biomass fractionation and upgrading of depolymerized products provide a renewable route for the production of fuels, chemicals, and materials.[1] Furfural, which can be readily produced *via* the acid-catalyzed dehydration of hemicellulose, is an important platform molecule for the preparation of solvents, fuels, drugs, and polymers.[2] The homocoupling of furfural *via* C–C bond formation delivers the long-chain products, which can serve as precursors for high-energy-density fuels and valuable chemicals.[3] The main pathways to achieve the homocoupling of furfural include benzoin condensation and pinacol coupling. Chen has pioneeringly performed the benzoin condensation of furfural and 5-hydroxylmethylfurfural using N-heterocyclic carbene as the catalyst under mild conditions.[4] The other mode of furfural homocoupling is pinacol coupling using reductants, during which expensive stoichiometric metals are typically used as reductants, generating hard-to-handle wastes. Recently, photochemical methods have been developed that enable the utilization of hydrazine, formate, and tertiary amines as reductants.[5] Alternatively, photoinduced electrons on semiconductors have also been identified as promising reagents to perform pinacol coupling.[6] The efficiency and product selectivity can be improved by engineering the exposed facets, modifying the surface hydroxyl groups, and increasing the surface oxygen vacancies.[7]

Ketones are useful building blocks in organic synthesis. The development of a method for the dehydroxylation of furoin into deoxyfuroin will expand the scope of furfural-derived products and inspire new applications of hemicellulose. However, the catalytic dehydroxylation of α-hydroxyl carbonyl compounds is challenging because the adjacent carboxyl group is also susceptible to reduction.[8] Normally, the derivatization of the hydroxyl group in benzoin is necessary to activate the C–O bond.[9] Sun *et al.* previously reported that deoxybenzoin can be obtained in the $ZnIn_2S_4$-photocatalyzed homocoupling of benzylic alcohol without the addition of sacrificial reagents, particularly in the presence of acid.[10] The dehydrogenative coupling of benzylic alcohol produces hydrobenzoin, which then undergoes dehydration to yield deoxybenzoin. However, the direct photocatalytic synthesis of deoxyfuroin from furoin has not yet been reported.

To expand the strategy for the semiconductor-photocatalyzed pinacol coupling of furfural and broaden the scope of furfural-derived products, we investigated the photocatalytic selective homocoupling of furfural to furoin on mesoporous TiO_2, followed by the direct deoxygenation of furoin to deoxyfuroin through the introduction of copper species into the mesoporous TiO_2 catalytic system. The mesopores modulated the structural and light absorption properties, influencing the product selectivity. It was found that only mesopores with a moderate size achieved the highest yield of furoin. Furthermore, the introduction of copper chloride into the mesoporous TiO_2-catalyzed system, as well as the combination of copper-loaded TiO_2 with HCl, efficiently promoted the deoxygenation of furoin.

To begin, we used Pluronic F127 (F127) as a template to introduce mesopores into TiO_2, thereby regulating its photocatalytic performance (Fig. 1 and Fig. S1, ESI†). Under light irradiation, the TiO_2 prepared without F127 produced a 26% yield of furoin **4**, and the main product was furfuryl alcohol **3** (42% yield). Both products **3** and **4** were photo-induced products. The 2-(diethoxymethyl)furan **2** was the acid-catalyzed condensation product between furfural and ethanol under dark conditions. The yield of furoin **4** increased with the amount of F127 (up to 0.4 g) used in the preparation of mesoporous TiO_2 ($mTiO_2$) with tetrabutyl titanate (2.1 g) and titanium tetrachloride (0.7 g) as precursors. Meanwhile, the formation of product **2** gradually decreased, which suggested that the dark reaction

[a] College of Chemistry, Zhengzhou University, Zhengzhou 450001, China. E-mail: hongjili@zzu.edu.cn
[b] School of Chemical Engineering, Zhengzhou University, Zhengzhou 450001, China. E-mail: lutianliang@zzu.edu.cn

† Electronic supplementary information (ESI) available. See DOI: https://doi.org/10.1039/d4cc06100d

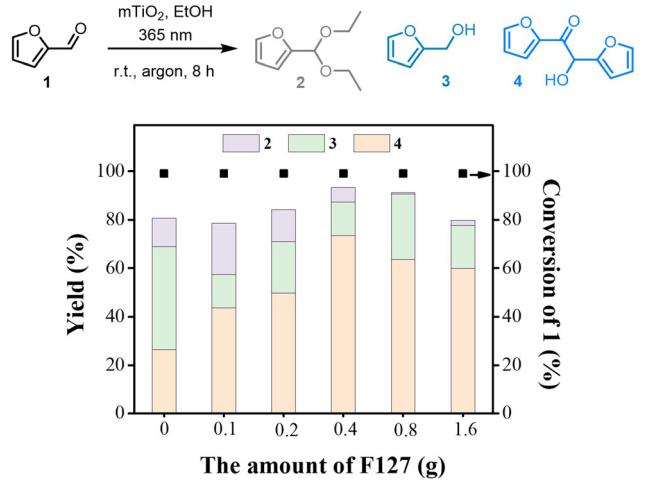

Fig. 1 Photocatalytic performance of mesoporous TiO_2 prepared with varying amounts of F127 as the template. Tetrabutyl titanate (2.1 g) and titanium tetrachloride (0.7 g) were used as Ti precursors in the synthesis of each mesoporous TiO_2 sample. Photocatalytic reaction conditions: catalyst (5 mg), furfural (30 mg), ethanol (2 mL), 365 nm LEDs, room temperature, argon, 8 h, gas chromatography (GC) yields.

was suppressed on $mTiO_2$. Further increasing the F127 amount (from 0.4 to 1.6 g) decreased the selectivity of product **4** and delivered more product **3**, indicating that the excess F127 affected the photocatalytic selectivity of $mTiO_2$. The optimal photocatalyst was $F127_{0.4}$-400-$mTiO_2$, which delivered a 73% yield of product **4** and a 14% yield of product **3**. This catalyst can be recycled three times without obvious deactivation (Fig. S2, ESI†).

To reveal the key factor induced by the usage of F127 during $mTiO_2$ preparation, structure and property characterizations were performed. Firstly, the powder X-ray diffraction (XRD) patterns of the samples indicated that all prepared catalysts belonged to anatase TiO_2 after 400 °C calcination (Fig. 2a). The nitrogen adsorption–desorption isotherms of the prepared samples were similar type-IV isotherms (Fig. 2b). The Barrett–Joyner–Halenda (BJH) pore-size distribution plots indicated that the formed pores belonged to mesopores, and the pore size continuously increased with the amount of F127 (Fig. 2c). Thus, a series of mesoporous TiO_2 with different pore sizes were successfully prepared through changing the amount of F127 template. The surface area of $mTiO_2$ was obviously increased through the introduction of mesopores (Fig. 2d). $F127_{0.8}$-400-$mTiO_2$ had the largest surface area of 131.5 $m^2\ g^{-1}$, compared to the $F127_0$-400-$mTiO_2$ (79.3 $m^2\ g^{-1}$). $F127_{0.4}$-400-$mTiO_2$ had a medium surface area of 104.1 $m^2\ g^{-1}$. Scanning electron microscopy (SEM) images indicated that these catalysts were formed by the aggregation of nanoparticles (Fig. 2e–g). The mean particle size of TiO_2 decreased from 17.6 to 12.0 nm after using F127 as the template, according to high-resolution transmission electron microscopy (HRTEM) images (Fig. 2h–j). $F127_{0.4}$-400-$mTiO_2$ has a medium particle size of 15.6 nm, and it showed a much better dispersion in solution than $F127_0$-400-$mTiO_2$ (Fig. S3, ESI†). The band gap of $mTiO_2$ increased with the amount of F127, and reached the maximum (2.93 eV) when the amount of F127 was 0.8 g (Fig. 2k). Further increasing the F127 amount to 1.6 g narrowed the band gap of $mTiO_2$. Thus, the redox capacity of $mTiO_2$ was affected by the F127 template. The photocurrent tests indicated the usage of F127 increased the photocurrent density of the catalyst (Fig. 2l), suggesting that these $mTiO_2$ had a better charge carrier separation efficiency.

Based on the above characterizations, it can be concluded that the F127 template used for $mTiO_2$ preparation introduced the mesopores and decreased the particle size, which further induced the increase of the surface area and charge-carrier separation efficiency, and the widening of the band gap. However, the photocatalytic performance did not always increase with these parameters. $F127_{0.4}$-400-$mTiO_2$ had mesopores with a moderate size, a moderate redox capacity and medium charge-carrier separation efficiency, showing the best performance in the photocatalytic coupling of furfural into furoin. The $mTiO_2$ samples with a smaller mesopore size had a narrow band gap, which may induce an inferior photocatalytic activity, leading to more formation of acetal byproduct **2**. The $mTiO_2$ samples with a larger mesopore size had a larger surface area, and showed a broad band gap or high charge carrier separation efficiency, which may induce the decrease in photocatalytic selectivity, leading to more formation of furfuryl alcohol byproduct.

Further investigation on other templates (Fig. S4, ESI†) also indicated that the moderate mesopore size ensured the good selectivity of furoin. Besides, higher or lower calcination temperature (Fig. S5, ESI†) induced an inferior catalytic performance due to transition of crystalline phase or template residue in the catalyst.

Controlled experiments were performed to reveal the reaction process. Firstly, a moderate amount of photocatalyst (5 mg) delivered the best yield of product **4**. A smaller amount of photocatalyst (2 mg) induced more product **2** from dark reactions (Fig. S6a, ESI†). A larger amount of photocatalyst promoted the formation of product **3**, suggesting that the presence of more photoinduced electrons may facilitate the deep reduction of **1** into **3**. Then, the effect of solvent was also studied (Fig. S6b, ESI†). During the photocatalytic reduction of furfural, the alcohol solvent acted as the electron sacrificial agent and hydrogen donor. It can be found that ethanol was the best solvent for furoin synthesis. Otherwise, the addition of water in ethanol dramatically switched the photocatalytic selectivity. The addition of water may decrease the solubility of the substrate and intermediates, and enhance their adsorption on the photocatalyst, which could induce the deep reduction of furfural into furfuryl alcohol. Thirdly, the time course of the photocatalytic reduction of furfural under optimal conditions was recorded (Fig. S6c, ESI†). The yield of product **4** had a linear increase with reaction time before 8 h. The product **2** was initially formed and then transformed into photoinduced products. The generation of product **3** was relatively lagging. In our previous reports on selectivity control in the photocatalytic reduction of aryl aldehydes, the concentration of aldehydes determined the single-electron or double-electron reduction pathway.[11] In the current system, the high furfural

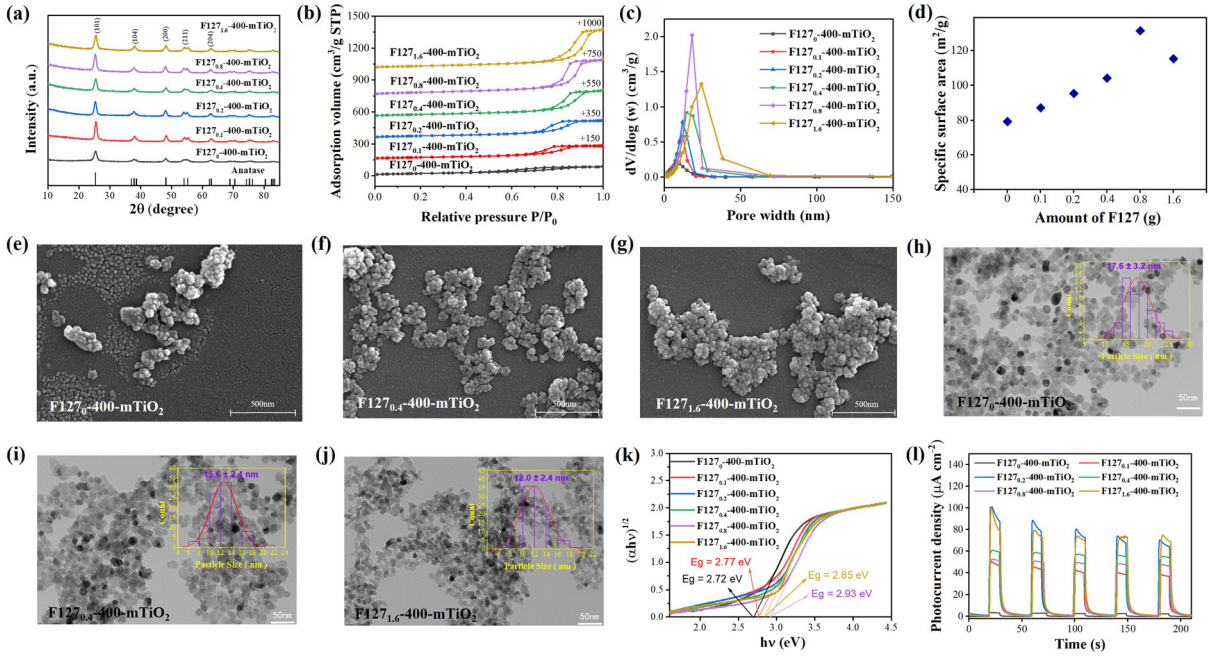

Fig. 2 Structure and property characterizations of mesoporous TiO_2 prepared using different amounts of F127 as the template. (a) XRD patterns. (b) Nitrogen adsorption–desorption isotherms. (c) Pore size distribution. (d) Specific surface area. (e)–(g) SEM images. (h)–(j) HRTEM images, and the insets are the size distribution of nanoparticles. (k) Kubelka–Munk function derived from UV-vis absorption spectra. (l) Transient photocurrent tests.

concentration at the initial stage could be beneficial for the single-electron reduction of furfural into furoin, and the low furfural concentration at a later period could promote the double-electron reduction of furfural into furfuryl alcohol.

The reaction mechanism can be proposed based on the above discussions and previous reports (Fig. S6d and e, ESI†).[12] Under light irradiation, the single-electron reduction of the formyl group of furfural could generate the carbon radical, which could undergo homocoupling into hydrofuroin or be reduced by the second electron into furfuryl alcohol. The hydrofuroin could be oxidized into furoin by the holes. The factors that can affect the generation of electrons on catalyst under light irradiation and the electron/substrate ratio could determine the reduction selectivity. The high surface area and high charge carriers separation efficiency of $mTiO_2$, and the high catalyst loading will induce a high electron/substrate ratio and promote the double-electron reduction of furfural into furfuryl alcohol. Only the moderate surface area and photochemical properties of $mTiO_2$ were beneficial for the single-electron reduction of furfural into furoin.

Further transformation of furoin will broaden the scope of furfural-derived products, however, the related reports are limited. Here, we investigated the photocatalytic dehydroxylation of furoin into deoxyfuroin (Fig. 3). 2-Propanol was used as the hydrogen donor and solvent. Meanwhile, dichloroethane was used as another solvent to dissolve the substrate. The $mTiO_2$ ($F127_{0.4}$-400-$mTiO_2$) without any cocatalysts only delivered a 12% yield of deoxyfuroin **5** (Fig. 3a). When copper halides were used as the cocatalysts, the yield of **5** was dramatically increased. Copper chloride was the best cocatalyst among the copper halides. The halide ions to coordinate copper were vital for this transfer hydrogenolysis reaction, as copper acetate and copper nitrate showed no promoting effect. Further increasing the amount of copper chloride delivered a 65% yield of **5** (Fig. 3a). The copper salts could be partially reduced and deposited on TiO_2 in the presence of 2-propanol. Then, the copper-loaded $mTiO_2$ ($Cu/mTiO_2$) was prepared *via* photo-deposition (Fig. S7 and S8, ESI†), and tested in the photocatalytic transfer hydrogenolysis of furoin (Fig. 3b). $Cu/mTiO_2$ showed a poor performance (Fig. 3b, entry 1), but the further addition of hydrogen chloride delivered a 62.1% yield of deoxyfuroin (Fig. 3b, entry 2 and Fig. S10, ESI†). The addition of other acid additives was invalid for the dehydroxylation reaction (Fig. S9, ESI†). The addition of HCl in the $Cu/mTiO_2$ system may induce the partial dissolution of the copper species. The sole $CuCl_2$ as photocatalyst also produced a 44% yield of deoxyfuroin (Fig. 3b, entry 3), and this reaction was photoinduced, as no reaction occurred under dark conditions (Fig. 3b, entry 4). These experiments suggested that the dissolved copper complex in 2-propanol should be one component of the photocatalytic species. Another photocatalytic species may be the loaded copper particle on $mTiO_2$. The TEM images (Fig. 3c) and Cu 2p X-ray photoelectron spectroscopy (XPS) analysis (Fig. 3d) demonstrated that the Cu_2O particle was deposited on $mTiO_2$ in the reaction system of $mTiO_2$ with $CuCl_2$ salt, and the Cu_2O particle was still partially reserved on $mTiO_2$ after the addition of HCl in the $Cu/mTiO_2$ system.[13] The initial addition of either the combination of $mTiO_2$ and $CuCl_2$ or the combination of $Cu/mTiO_2$ and HCl would generate the same photocatalytic species (Fig. 3e), which was the combination of the dissolved copper complex and copper particle loaded on $mTiO_2$. This hybrid system was the efficient photocatalyst for transfer hydrogenolysis of furoin into deoxyfuroin.

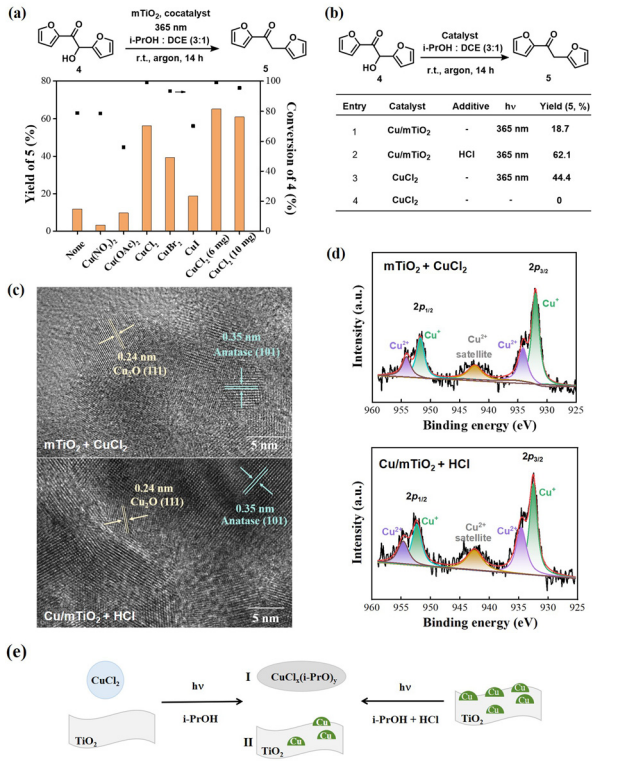

Fig. 3 Photocatalytic transfer hydrogenolysis of furoin to deoxyfuroin. (a) The effect of additives on the $mTiO_2$ photocatalyzed deoxygenation of furoin. Conditions: $F127_{0.4}$-400-$mTiO_2$ (10 mg), furoin (10 mg), additive (3 mg), solvent (1 mL), 365 nm LEDs, room temperature, argon, 14 h, GC yields. (b) Photocatalytic dehydroxylation of furoin using Cu-loaded $mTiO_2$ or $CuCl_2$ as the photocatalyst. Conditions: Cu/$F127_{0.4}$-400-$mTiO_2$ (10 mg) or $CuCl_2$ (2 mg), furoin (10 mg), HCl (37 wt%, 0 or 10 μL), solvent (1 mL), 365 nm LEDs, room temperature, argon, 14 h, GC yields. (c) TEM images, (d) Cu 2p XPS analysis, and (e) proposed generated copper species from the used $mTiO_2$ after reaction with the initial addition of $CuCl_2$ and the used Cu/$mTiO_2$ catalyst after reaction with the initial addition of HCl.

In conclusion, we developed a two-step photocatalytic reductive coupling of furfural into deoxyfuroin on mesoporous TiO_2. The using of F127 as a template for $mTiO_2$ preparation not only introduced the mesopores, but also decreased the $mTiO_2$ particle size, leading to a high surface area. The moderate redox ability and charge-carrier separation efficiency of $mTiO_2$ induced by the mesopores with a moderate size were conductive to the high selectivity of furoin during the photocatalytic transformation of furfural. Further addition of copper species in $mTiO_2$ to form the hybrid system composed of the dissolved copper species and loaded copper species efficiently photocatalyzed the dehydroxylation of furoin. This study enriched the surface engineering strategies for the photocatalytic pinacol coupling of furfural, and developed the photocatalytic method of direct synthesis of deoxyfuroin from furoin. However, further study is still needed to achieve higher product yields and reveal the mechanism of copper-catalyzed transfer hydrogenation.

We thank the National Natural Science Foundation of China (22109139, 22208315, 22379131) for funding support.

Data availability

The data supporting this article have been included as part of the ESI.†

Conflicts of interest

There are no conflicts to declare.

Notes and references

1 (*a*) M. Wang, H. Zhou and F. Wang, *Joule*, 2024, **8**, 604; (*b*) H. Li, A. Bunrit, N. Li and F. Wang, *Chem. Soc. Rev.*, 2020, **49**, 3748; (*c*) S. Feng, P. T. T. Nguyen, X. Ma and N. Yan, *Angew. Chem., Int. Ed.*, 2024, **63**, e202408504.
2 (*a*) C. Li, J. Li, L. Qin, P. Yang and D. G. Vlachos, *ACS Catal.*, 2021, **11**, 11336; (*b*) Y. Bao, Z. Du, X. Liu, H. Liu, J. Tang, C. Qin, C. Liang, C. Huang and S. Yao, *Green Chem.*, 2024, **26**, 6318; (*c*) H. Li, W. M. Chai, H. S. Luo and H. X. Li, *Chin. J. Chem.*, 2006, **24**, 1704; (*d*) C. Xu, L. Zheng, J. Liu and Z. Huang, *Chin. J. Chem.*, 2011, **29**, 691; (*e*) Z. Xia, Y. Li, J. Wu, Y.-C. Huang, W. Zhao, Y. Lu, Y. Pan, X. Yue, Y. Wang, C.-L. Dong, S. Wang and Y. Zou, *Sci. China: Chem.*, 2022, **65**, 2588.
3 (*a*) B. L. Wegenhart, L. Yang, S. C. Kwan, R. Harris, H. I. Kenttämaa and M. M. Abu-Omar, *ChemSusChem*, 2014, **7**, 2742; (*b*) H. Zang, K. Wang, M. Zhang, R. Xie, L. Wang and E. Y. X. Chen, *Catal. Sci. Technol.*, 1777, **2018**, 8; (*c*) M. Decostanzi, R. Auvergne, B. Boutevin and S. Caillol, *Green Chem.*, 2019, **21**, 724; (*d*) Z. Chen, J. Deng, Y. Zheng, W. Zhang, L. Dong and Z. Chen, *Chin. J. Catal.*, 2024, **61**, 135; (*e*) H. Wen, Z. Fan, S. Dou, J. C.-H. Lam, W. Zhang and Z. Chen, *Inorg. Chem. Front.*, 2024, **11**, 4449.
4 (*a*) L. Wang and E. Y. X. Chen, *ACS Catal.*, 2015, **5**, 6907; (*b*) L. Wang and E. Y. X. Chen, *Green Chem.*, 2015, **17**, 5149; (*c*) J. Wilson and E. Y. X. Chen, *ACS Sustainable Chem. Eng.*, 2016, **4**, 4927; (*d*) R. M. Cywar, L. Wang and E. Y. X. Chen, *ACS Sustainable Chem. Eng.*, 2018, **7**, 1980.
5 (*a*) Z. Qiu, H. D. M. Pham, J. Li, C.-C. Li, D. J. Castillo-Pazos, R. Z. Khaliullin and C.-J. Li, *Chem. Sci.*, 2019, **10**, 10937; (*b*) Q. Shen, K. Cao, X. Chen, X. Li, N. Zhang, Y.-B. Miao and J. Li, *Green Chem.*, 2023, **25**, 9665; (*c*) Y. Yan, G. Li, J. Ma, C. Wang, J. Xiao and D. Xue, *Green Chem.*, 2023, **25**, 4129.
6 L. Sun and N. Luo, *J. Energy Chem.*, 2024, **94**, 102.
7 (*a*) X. Wu, J. Li, S. Xie, P. Duan, H. Zhang, J. Feng, Q. Zhang, J. Cheng and Y. Wang, *Chem*, 2020, **6**, 3038; (*b*) R. Hu, W.-H. Xie, H.-Y. Wang, X.-A. Guo, H.-M. Sun, C.-B. Li, X.-P. Zhang and R. Cao, *Appl. Catal., B*, 2022, **304**, 120946; (*c*) Y. Jian, Y. Meng, J. Li, H. Wu, S. Saravanamurugan and H. Li, *J. Environ. Chem. Eng.*, 2022, **10**, 108837; (*d*) J. B. G. Filho, L. D. Almeida, H. F. V. Victória, G. H. M. Gomes, K. Krambrock, P. A. Robles-Azocar, M. C. Pereira and L. C. A. Oliveira, *J. Catal.*, 2024, **436**, 115580.
8 X. Xu, L. Yan, Z.-K. Zhang, B. Lu, Z. Guo, M. Chen and Z.-Y. Cao, *Molecules*, 2022, **27**, 4675.
9 (*a*) E. Speckmeier, C. Padié and K. Zeitler, *Org. Lett.*, 2015, **17**, 4818; (*b*) J. Zhang, J.-D. Yang and J.-P. Cheng, *Chem. Sci.*, 2020, **11**, 8476.
10 G. Han, X. Liu, Z. Cao and Y. Sun, *ACS Catal.*, 2020, **10**, 9346.
11 H. Fu, H. Chen, B. Gao, T. Lu, Y. Su, L. Zhou, M. Liu, H. Li and X. Yang, *ChemCatChem*, 2022, **14**, e202200120.
12 (*a*) H. Li, Z. Gao, L. Lei, H. Liu, J. Han, F. Hong, N. Luo and F. Wang, *Green Chem.*, 2020, **22**, 3802; (*b*) Z. Peng, Z. Wu, X. Sun and H. Li, *Green Chem.*, 2023, **25**, 6869.
13 M. Liu, H. Li, J. Zhang, H. Liu and F. Wang, *Angew. Chem., Int. Ed.*, 2023, **63**, e202315795.

